Nanoscale
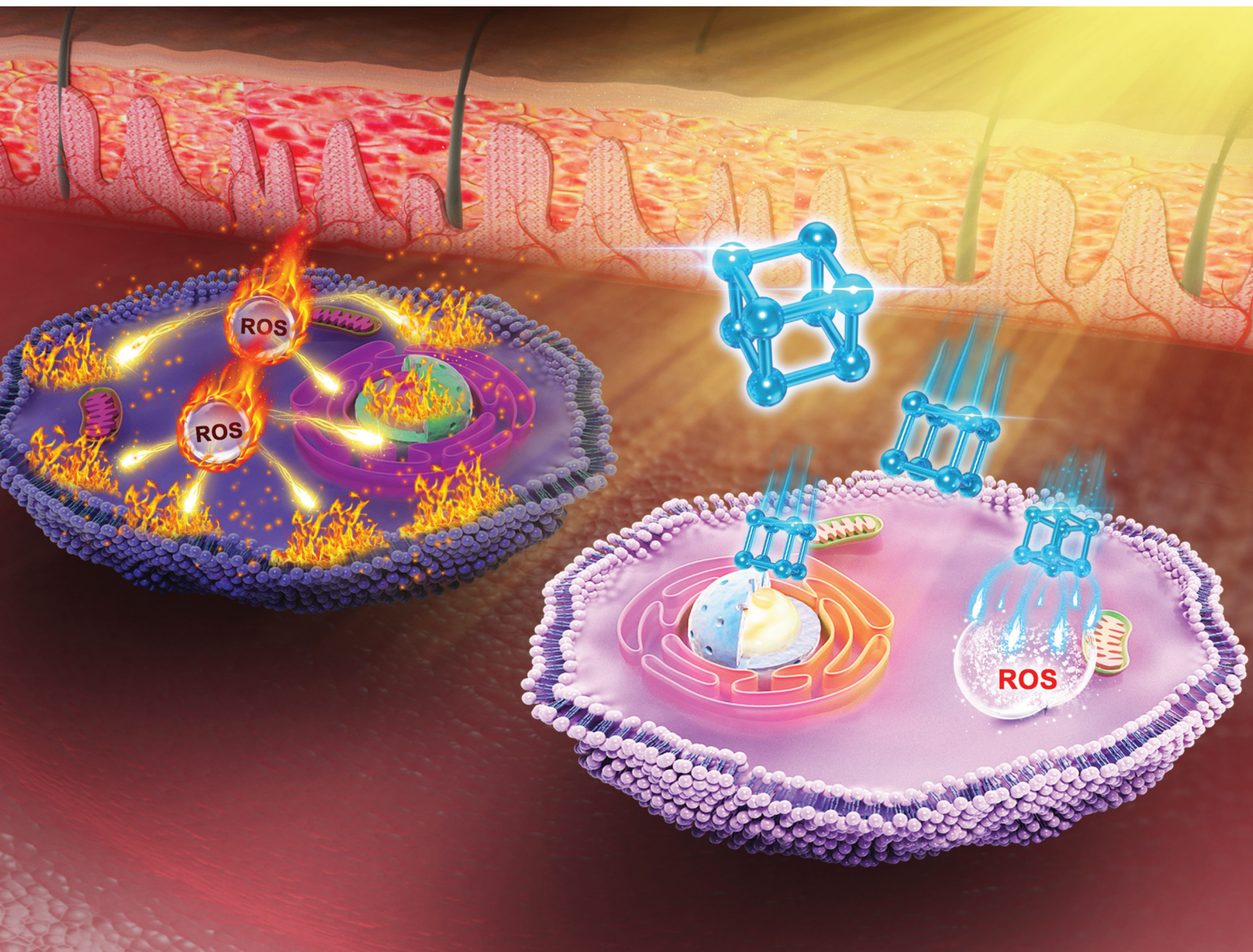
ROYAL SOCIETY
OF CHEMISTRY

PAPER
Ning Gu, Dan Luo *et al.*
Ultrasmall Prussian blue nanoparticles attenuate UVA-induced cellular senescence in human dermal fibroblasts *via* inhibiting the ERK/AP-1 pathway

NCNST

Nanoscale

PAPER

Check for updates

Ultrasmall Prussian blue nanoparticles attenuate UVA-induced cellular senescence in human dermal fibroblasts *via* inhibiting the ERK/AP-1 pathway

Yueyue Li, [ID] [a] Ni Zeng,[a] Zhiguo Qin,[b] Yihe Chen,[a] Qian Lu,[a] Yuxin Cheng,[a] Qingyue Xia,[a] Zhiyu Lu,[a] Ning Gu*[b] and Dan Luo*[a]

Ultraviolet A (UVA) irradiation can induce cellular senescence and cause skin photoaging, which is mainly driven by the excessive production of reactive oxygen species (ROS). Emerging studies have focused on new strategies for the prevention of skin photoaging. Ultrasmall Prussian blue nanoparticles (USPBNPs) demonstrate an intensive ability to scavenge ROS as nanozymes and exhibit great potential in the treatment of ROS-related diseases. Our goal was to investigate the anti-senescent role of USPBNPs against UVA-induced premature senescence in human dermal fibroblasts (HDFs). Our results showed that the activation of senescence-associated β-galactosidase (SA-β-gal) and the arrest of the cell cycle induced by UVA radiation in HDFs were significantly inhibited by pretreatment of USPBNPs (1 μg mL^{-1}). Furthermore, USPBNPs downregulated the expression of DNA damage marker γH2AX and inhibited the secretion of senescence-associated secretory phenotypes (SASP) including IL-6, TNF-α and matrix metalloproteinases (MMPs). In addition, we found that the antiphotoaging effect of USPBNPs involved the scavenging of ROS as well as the inhibition of the ERK/AP-1 pathway. In conclusion, USPBNPs exhibited great potential to become novel anti-photoaging agents by alleviating UVA-induced cellular senescence and thus delaying the process of skin photoaging.

1. Introduction

Skin aging, which consists of intrinsic aging and extrinsic aging, is characterized by wrinkles, dryness, dyspigmentation and susceptibility to cancer.[1,2] UV radiation is the main factor that causes extrinsic aging, which is also known as photoaging.[3] There are three types of UV radiation based on the wavelengths, namely UVA, UVB and UVC.[4] While UVC is completely absorbed by the atmosphere, UVA and UVB can reach the ground.[2] Compared to UVB, UVA can penetrate more deeply into the dermis and thus become the main factor leading to skin photoaging.[2] UVA radiation can stimulate the production of ROS and indirectly induce oxidative damage to the DNAs, proteins and lipids.[5] Moreover, increased ROS could promote extracellular signal-regulated kinases (ERK) phosphorylation and subsequently stimulate the transcriptional activity of activator protein-1 (AP-1), which consists of c-Jun and c-Fos.[4] AP-1 further upregulates MMP expression and results in the pro-

gress of photoaging.[4,6,7] In response to UV radiation, cells can enter a state of stable arrest in the cell cycle called cellular senescence,[8,9] which is mediated by the p16^{INK4A}/pRb and p53/p21^{WAF1} pathways.[10–12] In addition to the cell cycle arrest, senescent cells exhibit increased SA-β-gal activity[13] and undergo persistent DNA damage response that can be reflected by the DNA damage response protein γH2AX.[14,15] Moreover, senescent cells will secrete more SASP including cytokines, proteases and growth factors.[4,16] For skin, cellular senescence is not only a feature of aging, but also an important mechanism to mediate aging.[17,18] Hence, the regulation of the ROS level is an important strategy to prevent UVA-induced cellular senescence and photoaging.[1]

Nanozymes are nanomaterial-based enzymes with higher catalytic stability and lower manufacturing cost in comparison with protein enzymes.[10,19,20] By effectively regulating the ROS balance,[21] nanozymes have been successfully applied in the treatment of diverse diseases, such as pancreatic cancer, brain injury, Parkinson's disease and pneumonia.[22–24] Prussian blue (PB) is an iron-based metal–organic framework and is considered to be a promising coordination polymer for theranostics.[25] In recent years, Prussian blue nanoparticles (PBNPs) demonstrated efficient ability to remove excessive ROS by mimicking multiple enzymes and showed a novel therapeutic

*a*Department of Dermatology, The First Affiliated Hospital of Nanjing Medical University, Nanjing 210029, China. E-mail: daniluo2005@163.com
*b*State Key Laboratory of Bioelectronics, Jiangsu Key Laboratory for Biomaterials and Devices, School of Biological Science and Medical Engineering, Southeast University, Nanjing 210096, China. E-mail: guning@seu.edu.cn

role in skin wound healing, acute pancreatitis and anemia.[26–30] However, PBNPs still have shortcomings such as a relatively large size and weak catalytic activity. Fortunately, USPBNPs with a size of about 3.4 nm were successfully synthesized in our previous study, which exhibited a more intensive ability to scavenge ROS.[31] The present work aimed to study whether USPBNPs could attenuate UVA-induced cellular senescence in HDFs so as to prevent the progress of photoaging. Our results indicated that USPBNPs exhibit a notable effect on anti-cellular senescence by scavenging ROS and inhibiting the ERK/AP-1 pathway in UVA irradiated HDFs, which may become novel, efficient antiphotoaging agents.

2 Experimental methods

2.1 Synthesis and characterization of USPBNPs

In brief, USPBNPs were obtained by dissolving 0.0275 g of K3[Fe-(CN)6] in 10 mL of 75% ethanol solution with 0.75 g of polyvinyl pyrrolidone (PVP) and 0.01 M hydrochloric acid. Then, the solution was reacted at 80 °C for 3 h and cooled to room temperature before purification. A JEM-2100 transmission electron microscope (TEM, JEOL, Japan) was used to observe the microstructure and particle size of USPBNPs. An X-ray diffraction analyzer (XRD, Thermo X'TRA, USA) was used to test the crystalline phases of USPBNPs. The ultraviolet–visible (UV–vis) absorption spectrum of USPBNPs was obtained using a UV-vis-NIR spectrophotometer (UV-3600, Shimadzu, Japan).

2.2 Cell culture and UVA radiation

To isolate HDFs, the foreskin from donors were rinsed with normal saline and immersed in iodophor for 10 min. Then, the subcutaneous tissues of the foreskin were removed using ophthalmic tweezers. The remaining foreskin were incubated with 0.5% dispase at 37 °C for 2 h to separate the epidermis and dermis. Next, the dermis was digested with 0.2% collagenase at 37 °C for 2 h and the suspension was filtered and centrifuged. Finally, the supernatants were discarded and the remaining HDFs were incubated in a high-glucose DMEM medium (Gibco, Life Technologies, USA) with 10% FBS and antibiotics. Cells in the logarithmic growth phase from passages 3–9 were used for our experiments. The following subgroups were set: the control group without USPBNPs treatment or UVA radiation, the UVA group with UVA radiation and the USPBNPs + UVA group that was pretreated with USPBNPs for 24 h before UVA radiation. UVA radiation was delivered using UVA phototherapy instruments (Sigma, Shanghai, China) which emitted UVA at a wavelength of 320–400 nm. The medium was removed before UVA irradiation and replaced with a thin film of PBS. Then, HDFs were exposed to UVA radiation at a distance of 15 cm between the UVA phototherapy instruments and the cell culture dish.

2.3 Cell viability assay

A cell counting kit-8 (CCK-8, Bimake, Shanghai, China) was used to determine the cell viability of HDFs in different groups according to the manufacturer's instructions. In brief, HDFs
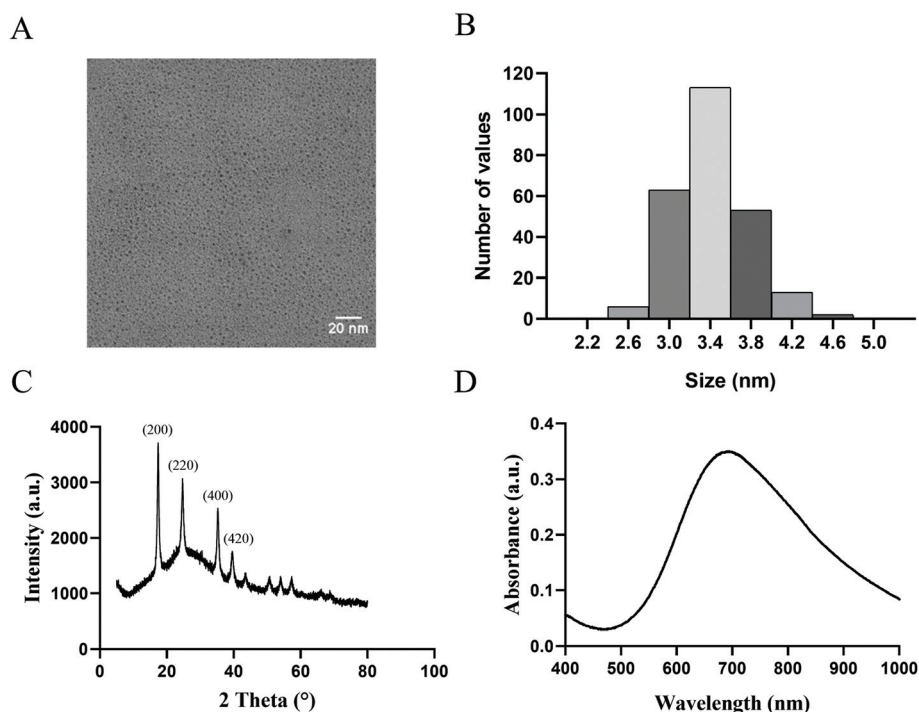

Fig. 1 Characterization of USPBNPs. (A) Representative TEM image of USPBNPs; scale bar: 20 nm. (B) The size distribution of USPBNPs under TEM. (C) XRD pattern of USPBNPs. (D) UV–visible absorbance spectra of USPBNPs.

were incubated at a density of 2×10^3 and five parallel wells were used for each group. After different treatments and incubation for 24 h, HDFs in each well were added with the CCK-8 solution and incubated for 2 h. Finally, the optical density, which reflects cell proliferation, was measured at 450 nm using a spectrophotometer.

2.4 Senescence-associated β-galactosidase (SA-β-gal) staining

The activity of SA-β-gal was analyzed using a senescence β-galactosidase staining kit (Cell Signaling Technology, CST, MA, USA). First, HDFs were rinsed with PBS and fixed at room temperature for 15 min. Then, the β-gal staining solution was added and HDFs were cultured at 37 °C in a dry incubator overnight. Finally, the blue colored cells were counted under a microscope when β-galactosidase is still on the plate.

2.5 Cell cycle analysis

HDFs in different groups were collected at 24 h after various treatments and stained with the DNA staining solution using a cell cycle staining kit (MultiSciences, Hangzhou, China) in accordance with the manufacturer's instructions. After incubation at room temperature with protection from light for 30 min, HDFs in different groups were analyzed using a flow cytometer.

2.6 Western blotting

HDFs in various groups were lysed with the RIPA buffer (Thermo Fisher Scientific, USA) which contains PMSF (Beyotime Biotechnology, Shanghai, China) and a phosphatase inhibitor (Beyotime Biotechnology, Shanghai, China). The protein samples in various groups were electrophoresed in 10% SDS/PAGE gels and transferred to PVDF membranes (Millipore, Bedford, MA). The membranes were then incubated in tris-buffered saline tween (TBST) with 5% nonfat milk. The following primary antibodies were used, including anti-p16 (CST), anti-p21(CST), anti-p53 (CST), anti-IL-6 (Abcam), anti-TNF-α (Proteintech), anti-MMP-1 (Proteintech), anti-MMP-3 (Proteintech), anti-MMP-9 (Proteintech), anti-γH2AX (CST), anti-p-ERK (CST), anti-ERK (CST), anti-c-Jun (CST), anti-c-Fos (CST) and anti-GAPDH (CST). The PVDF membranes were then washed with TBST and incubated with HRP-conjugated goat anti-mouse or peroxidase-conjugated goat anti-rabbit secondary antibodies. Finally, the protein bands were observed using enhanced ECL reagents and a chemiluminescent detection system.
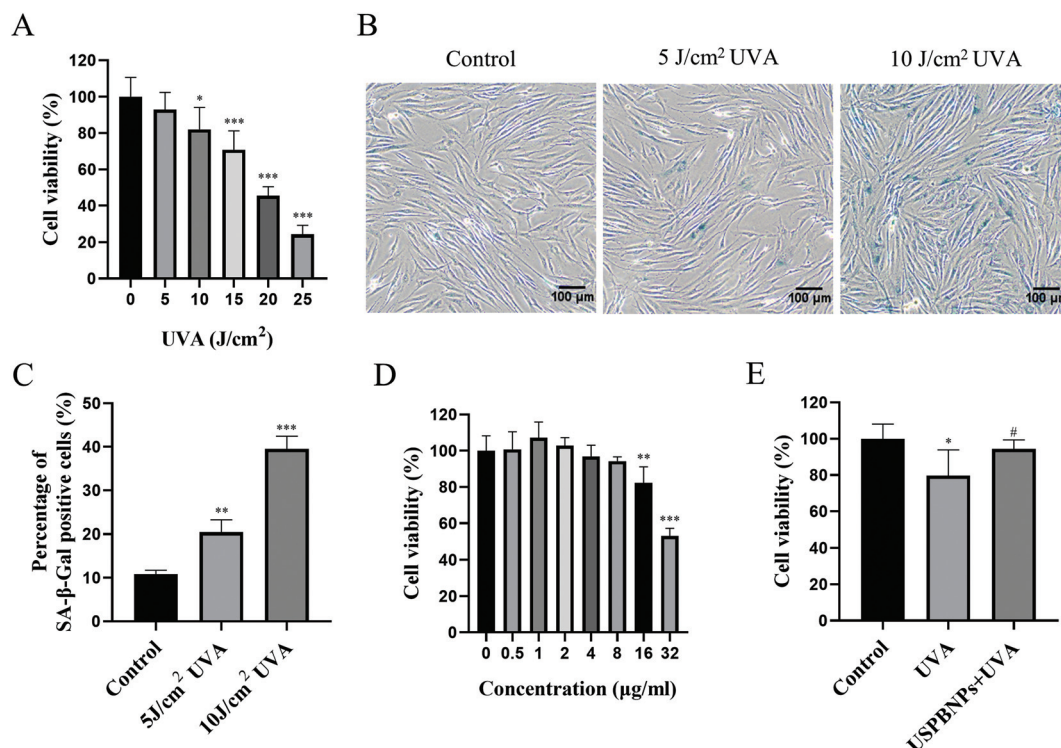

Fig. 2 Optimization of UVA dosage and USPBNP concentration. (A) Cell viability of HDFs at 24 h after different doses of UVA irradiation (5–25 J cm^{-2}) detected using the CCK-8 assay. (B) SA-β-gal staining of HDFs at 24 h after 5 and 10 J cm^{-2} UVA radiation; scale bar: 100 μm. (C) Percentage of SA-β-gal positively stained cells calculated by Image J. (D) Cell viability of HDFs after 24 h of treatment with different concentrations of USPBNPs (0.5–32 μg ml^{-1}) analyzed using the CCK-8 assay. (E) Cell viability of HDFs at 24 h after UVA irradiation with or without USPBNPs pretreatment detected using the CCK-8 assay. *$P < 0.05$, **$P < 0.01$, and ***$P < 0.001$ *versus* the control group; #$P < 0.05$ *versus* the UVA group.

2.7 Quantitative real-time PCR (q-RT PCR)

HDFs in various groups were collected and the total RNA of HDFs was extracted using an RNA isolation kit (Vazyme Biotech, Nanjing, China). Then, RNA was reverse transcribed into cDNA using a reverse transcriptase kit (Vazyme Biotech, Nanjing, China). The mRNA expressions of representative SASP which were normalized to GAPDH were detected by q-RT PCR. Each RNA level was quantified using the 2-ΔΔCt method. Primers used in the present study were as follows:

IL-6, 5′-ACTCACCTCTTCAGAACGAATTG-3′,
5′-CCATCTTTGGAAGGTTCAGGTTG-3′;
TNF-α, 5′-CCTCTCTCTAATCAGCCCTCTG-3′,
5′-GAGGACCTGGGAGTAGATGAG-3′;

MMP1, 5′-CAGATGCTGAAACCCTGAA-3′,
5′-CAGATGTGTTTGCTCCCA-3′;
MMP3, 5′-CGGTTCCGCCTGTCTCAAG-3′,
5′-CGCCAAAAGTGCCTGTCTT-3′;
MMP9, 5′-GGGACGCAGACATCGTCATC-3′,
5′-TCGTCATCGTCGAAATGGGC-3′;
GAPDH, 5′- GGGGCTCTCCAGAACATC-3′,
5′-TGACACGTTGGCAGTGG-3′.

2.8 Intracellular ROS analysis

The intracellular ROS level was detected using a ROS assay kit (Beyotime Biotechnology, Shanghai, China). Briefly, HDFs were collected at 24 h after different treatments and incubated with DCFH-DA. After incubation for 20 min, HDFs were washed and
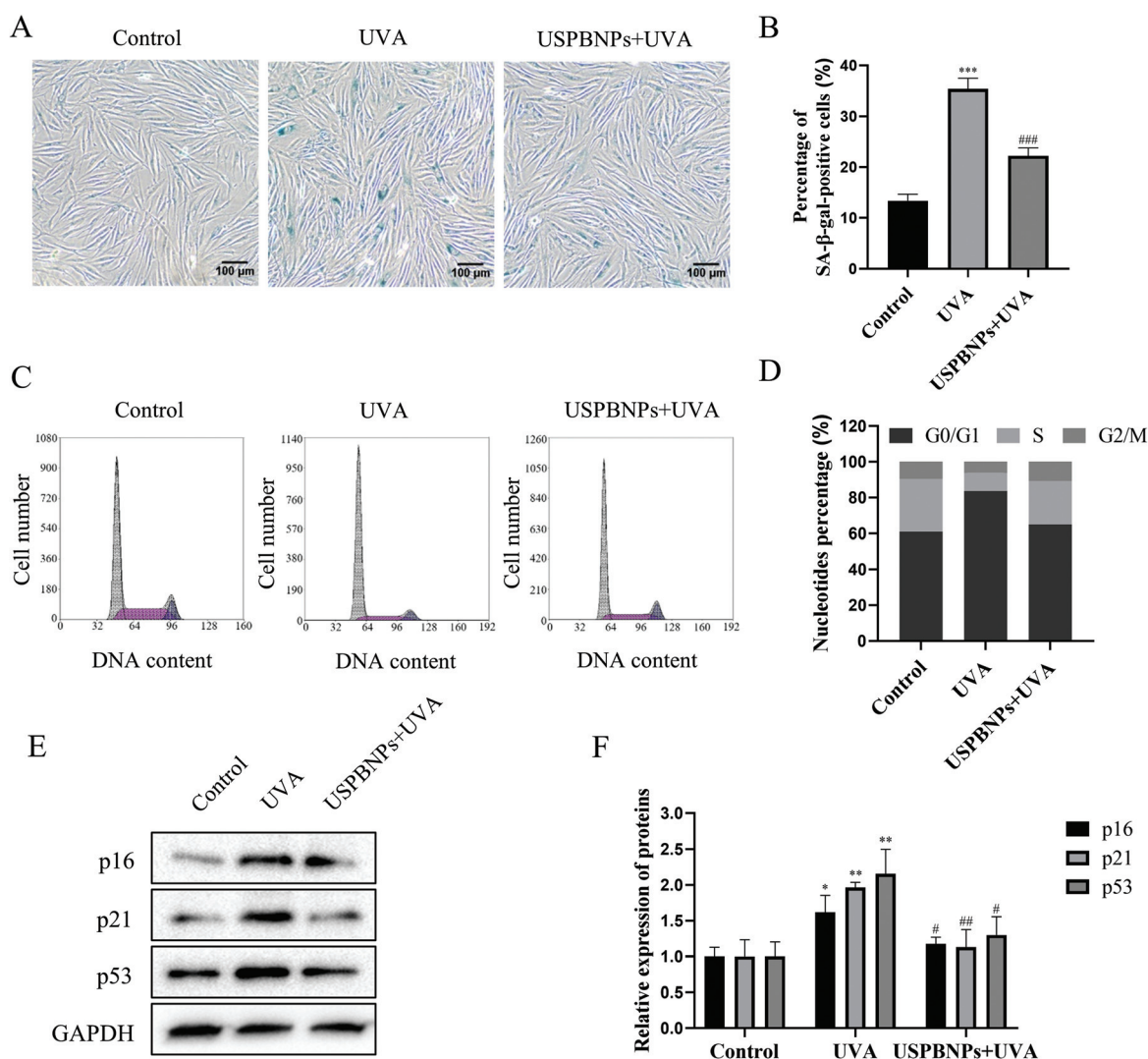

Fig. 3 USPBNPs decreased the SA-β-gal activity, attenuated the cell cycle arrest and reduced the expressions of p16, p21 and p53 in UVA-irradiated HDFs. (A) SA-β-gal staining of HDFs at 24 h after UVA irradiation with or without USPBNP pretreatment; scale bar: 100 μm. (B) Percentage of SA-β-gal positively stained cells calculated by Image J. (C) Cell cycle analysis of HDFs at 24 h after UVA irradiation with or without USPBNPs pretreatment by flow cytometry. (D) Cell cycle distribution in each group. (E) The protein levels of p16, p21 and p53 in HDFs at 24 h after UVA irradiation with or without USPBNP pretreatment detected by western blot. (F) Quantification of the western blot band signals of p16, p21 and p53 by Image J. $*P < 0.05$, $**P < 0.01$, and $***P < 0.001$ *versus* the control group; $^{\#}P < 0.05$, $^{\#\#}P < 0.01$ and $^{\#\#\#}P < 0.001$ *versus* the UVA group.

suspended in PBS. The relative ROS level was detected using a flow cytometer (Beckman Coulter, CA, USA) and a confocal laser scanning microscope (Leica Stellaris 8, Germany).

2.9 Immunofluorescence imaging of γH2AX

HDFs in different groups were fixed using 4% paraformaldehyde (PFA) and permeabilized using 0.5% Triton x-100. Then, HDFs were blocked with 5% BSA and incubated with the anti-γH2AX antibody (1 : 800, CST) at 4 °C overnight. On the next day, HDFs were incubated with the Cy™ 3-conjugated goat anti-rabbit antibody (1 : 200) for 1 h at room temperature. Then, nuclei of HDFs were stained by DAPI at room temperature for 5 min. Finally, Fluorescent images of HDFs were captured under a confocal microscope (Nikon A1R HD, Japan).

2.10 Statistical analysis

All experiments were conducted at least three times and data were presented as mean ± SD. Differences between groups were evaluated by Student's t-test using GraphPad Prism. A P value of <0.05 was considered statistically significant.

3 Results and discussion

3.1 Preparation and characterization of USPBNPs

USPBNPs were prepared using 75% ethanol as the solvent and PVP as the capping agent as previously described.[31] The size of USPBNPs was about 3.4 nm on average based on the TEM observation (Fig. 1A and B). X-ray powder diffraction (XRD)
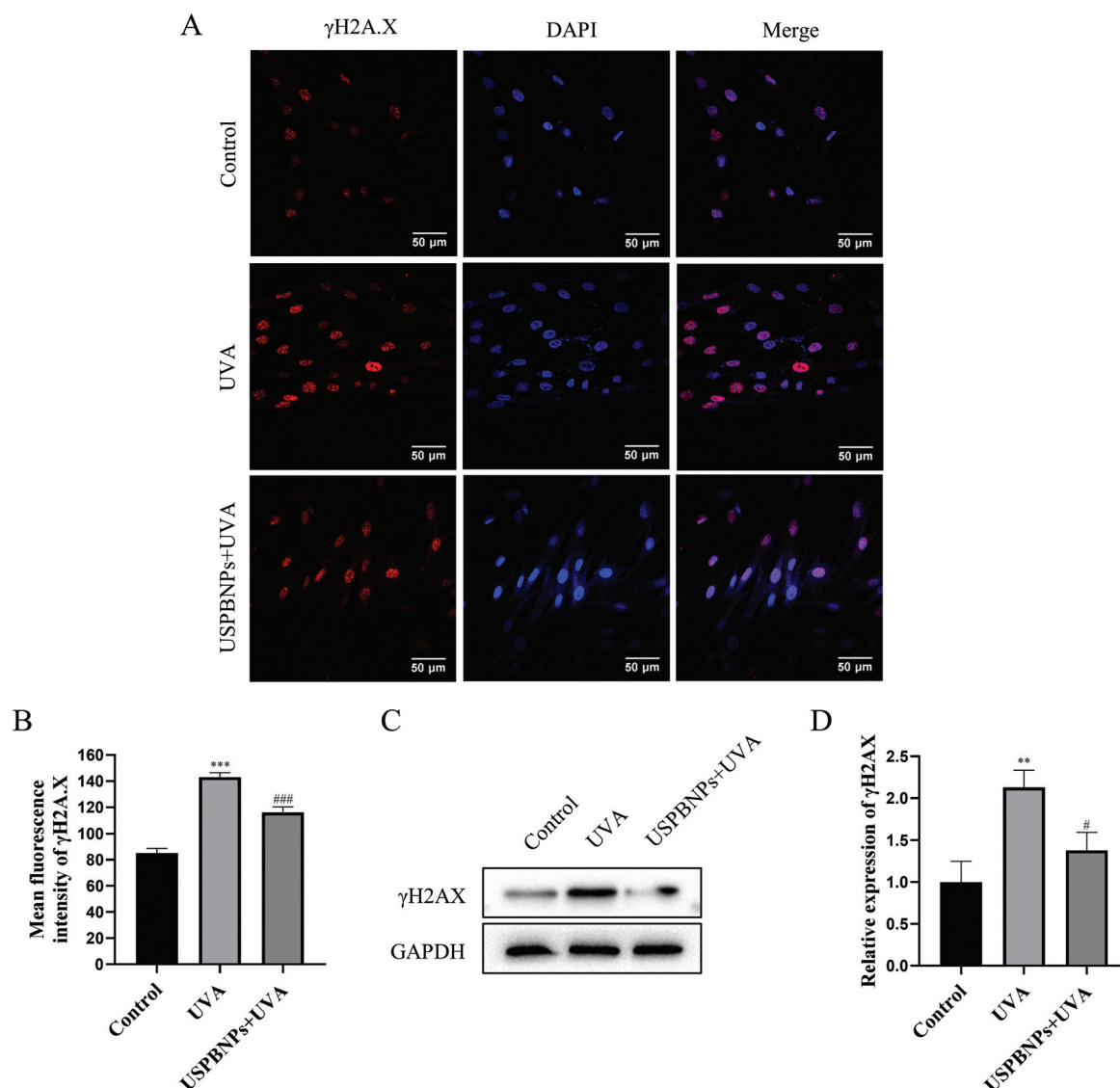

Fig. 4 USPBNPs decreased the γ-H2AX expression in UVA-irradiated HDFs. (A) Immunofluorescence staining of γ-H2AX (red) and DAPI (blue) in HDFs at 24 h after UVA irradiation with or without USPBNPs pretreatment observed under a confocal microscope; scale bar: 20 μm. (B) Quantification of mean γ-H2AX fluorescence intensity by Image J. (C) The protein expression of γ-H2AX in HDFs at 24 h after UVA irradiation with or without USPBNP pretreatment detected by western blot. (D) Quantification of the western blot band signals of γ-H2AX by Image J. **$P < 0.01$ and ***$P < 0.001$ *versus* the control group; #$P < 0.05$ and ###$P < 0.001$ *versus* the UVA group.

revealed that USPBNPs had characteristic diffraction peaks at $17.5°$ (200), $24.6°$ (220), $35.2°$ (400), and $39.5°$ (420), which demonstrated the crystal phase purity of the USPBNPs (Fig. 1C). The absorption spectra of USPBNPs (Fig. 1D) displayed a characteristic absorbance peak at 697.5 nm, which was caused by electron transition between $Fe(II)$ and $Fe(III)$. Taken together, USPBNPs with ultrasmall size and high crystallinity were successfully synthesized.

3.2 Optimization of UVA dosage and USPBNP concentration

To establish the cellular senescence model of HDFs, the effects of 5, 10, 15, 20 and 25 J cm^{-2} UVA radiation for HDFs were initially accessed. As demonstrated in Fig. 2A, the viability of HDFs was significantly diminished to a relatively low level when the dosage of UVA radiation reached 15 J cm^{-2} compared with the control group, so we proceeded using 5 and 10 J cm^{-2} UVA for further investigations. As activation of SA-β-gal is a critical characteristic of cellular senescence,[13] the SA-β-gal activity in HDFs among different groups was then investigated. As shown in Fig. 2B and C, SA-β-gal positively stained cells significantly outnumbered in 5 J cm^{-2} and 10 J cm^{-2} UVA-irradiated HDFs than in non-irradiated HDFs. Moreover, the percentage of positively stained cells in the 10 J cm^{-2} UVA group was markedly higher than that in the 5 J cm^{-2} UVA group. Therefore, 10 J cm^{-2} UVA radiation was ultimately selected for the cellular senescence model. Next, we evaluated the cytotoxic effect of USPBNPs on HDFs in the concentration range of 0.5 μg ml^{-1} to 32 μg ml^{-1} to determine the optimal concentration. As shown in Fig. 2D, no cytotoxic effects were observed in HDFs following treatment with USPBNPs with the concentration ranging from 0.5 μg ml^{-1} to 8 μg ml^{-1} compared to the control group. Moreover, a relatively low concentration of USPBNPs (1 μg ml^{-1}) demonstrated the strongest ability to promote cell proliferation, although the data were not statistically significant. We further found that 1 μg ml^{-1} USPBNPs could significantly promote cell proliferation in UVA irradiated HDFs, which indicated its photoprotective role against UVA irradiation (Fig. 2E). Based on the above observation, 1 μg ml^{-1} USPBNPs were utilized in the subsequent experiments. It should be noted that the dose of USPBNPs in the present study was much lower than that of PBNPs used in previously published studies,[26,29,30] which can be attributed to its ultrasmall size.

3.3 USPBNPs decrease the SA-β-gal activity in UVA-irradiated human dermal fibroblasts

To investigate the effect of USPBNPs on cellular senescence caused by UVA radiation, we first examined the SA-β-gal activity among different groups. Fig. 3A and B show that positively stained cells were much more in UVA-irradiated HDFs in comparison with non-irradiated HDFs. However, this increase of the SA–β-gal activity was reversed by USPBNPs as positively stained cells were significantly reduced in USPBNP-pretreated HDFs. Thus, our data demonstrated that USPBNPs ameliorated UVA-induced cellular senescence in HDFs by decreasing the SA-β-gal activity.
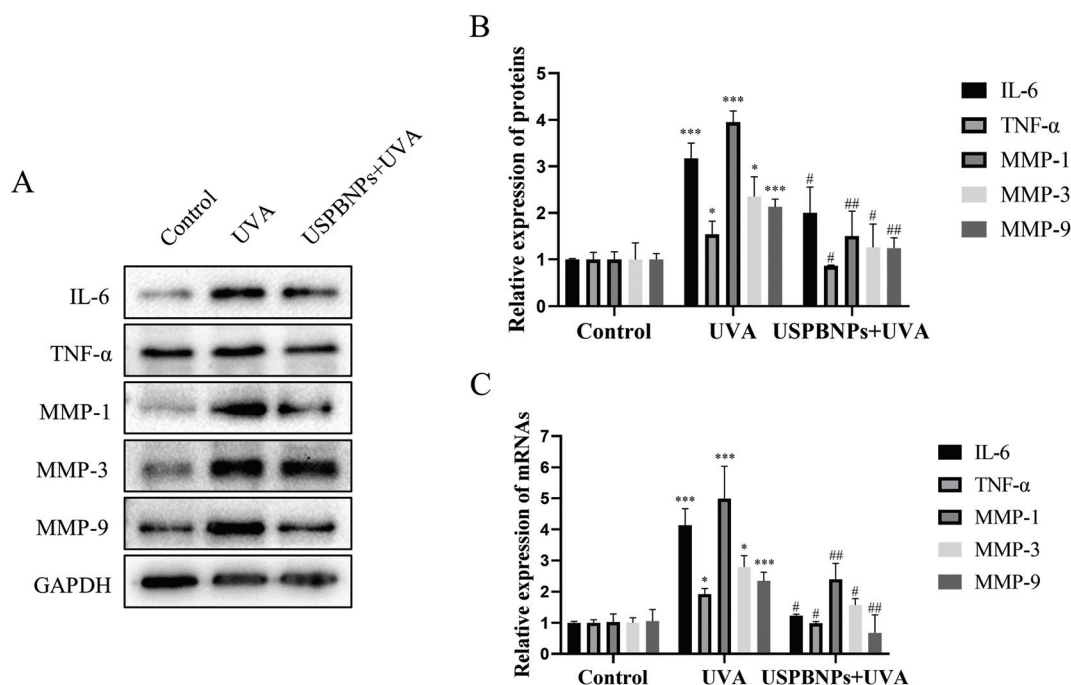

Fig. 5 USPBNPs inhibited the expressions of SASP in UVA-irradiated HDFs. (A) The protein expressions of IL-6, TNF-α and MMPs in HDFs at 24 h after UVA irradiation with or without USPBNP pretreatment detected by western blot. (B) Quantification of the western blot band signals in (A) by Image J. (C) Relative mRNA expressions of IL-6, TNF-α and MMPs in HDFs at 24 h after UVA irradiation with or without USPBNP pretreatment by qRT-PCR. $*P < 0.05$ and $***P < 0.001$ versus the control group; $\#P < 0.05$ and $\#\#P < 0.01$ versus the UVA group.

3.4 USPBNPs attenuate the G1/S phase cell cycle arrest and decrease the expressions of senescence associated proteins in UVA-irradiated human dermal fibroblasts

It is known that cell cycle arrest is a basic feature of cellular senescence.[17] The effect of USPBNPs on the cell cycle distribution of UVA irradiated HDFs was assessed using a cell cycle kit. The results showed an obvious increase in the G1 phase of HDFs after UVA irradiation, while cells in the S phase were decreased, indicating the cell cycle arrest in G1/S transition. Interestingly, the pretreatment of USPBNPs inhibited the G1/S phase block induced by UVA radiation (Fig. 3C and D). Moreover, we detected the expression level of senescence associated proteins including p16, p21 and p53 in HDFs by western blot. As shown in Fig. 3E and F, the protein level of p16, p21 and p53 in HDFs was significantly upregulated after UVA radiation, while pretreatment of USPBNPs significantly diminished the expressions of these proteins. Our results demonstrated that USPBNPs could alleviate the G1/S phase cell cycle arrest induced by UVA radiation in HDFs by downregulating the expressions of p16, p21 and p53.

3.5 USPBNPs reduce γ-H2AX expression in UVA-irradiated human dermal fibroblasts

Increased expression of γH2AX foci in the nuclei has been reported to become a biomarker of cellular senescence.[15,17]
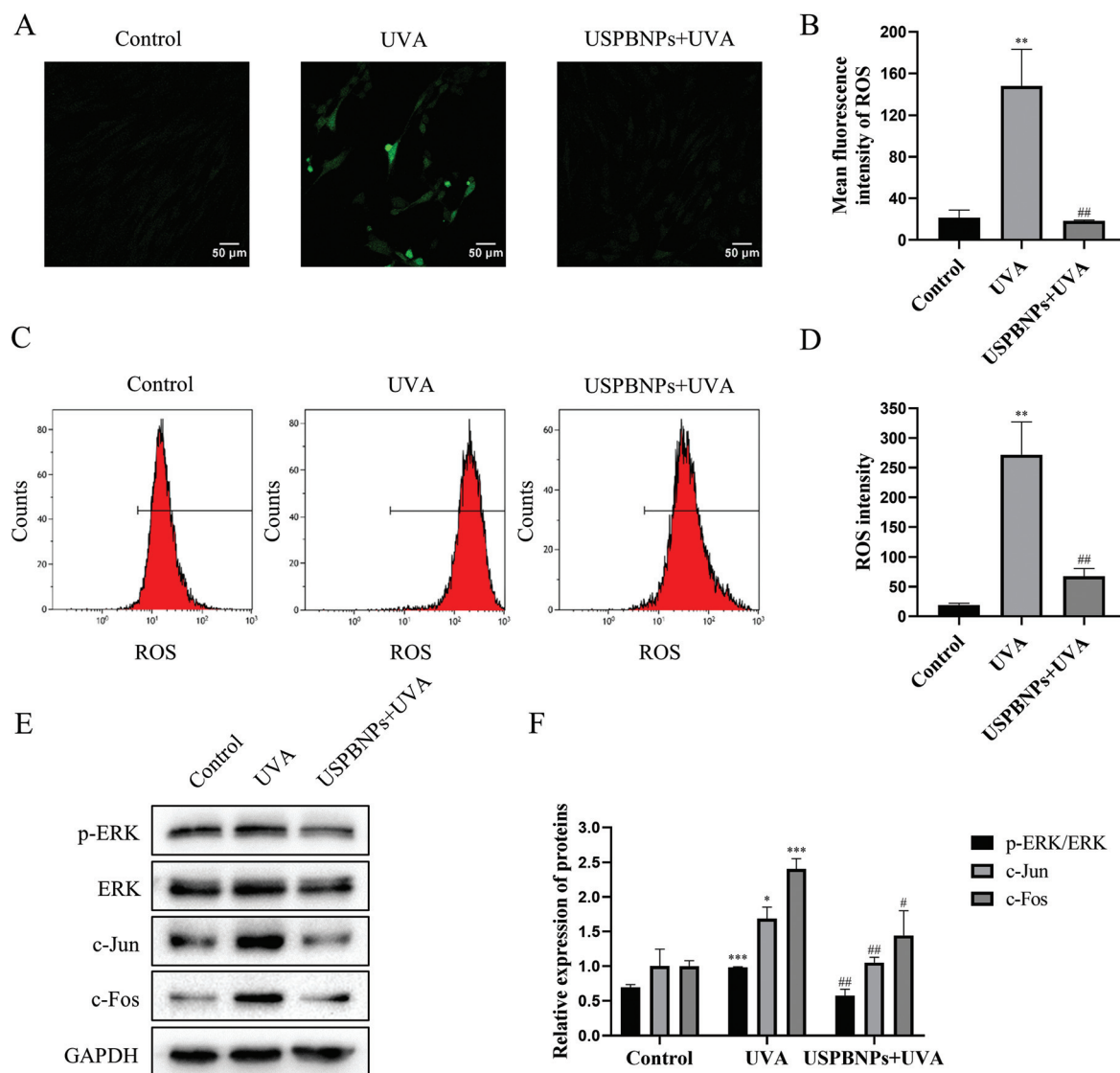

Fig. 6 USPBNPs decreased the intracellular ROS level and inhibited the ERK/AP-1 pathway in UVA-irradiated HDFs. (A) Representative images of intracellular ROS (green) in HDFs at 24 h after UVA irradiation with or without USPBNP pretreatment observed under a confocal microscope; scale bar: 100 μm. (B) Quantification of mean ROS fluorescence intensity by Image J. (C) ROS generation in HDFs at 24 h after UVA irradiation with or without USPBNP pretreatment by flow cytometry analysis. (D) Quantitative analysis of ROS intensity data from flow cytometry analysis. (E) The protein level of p-ERK, ERK, c-Jun and c-Fos in HDFs at 24 h after UVA irradiation with or without USPBNP pretreatment detected by western blot. (F) Quantification of the western blot band signals in (E) by Image J. *$P < 0.05$, **$P < 0.01$ and ***$P < 0.001$ *versus* the control group; #$P < 0.05$ and ##$P < 0.01$, *versus* the UVA group.

Therefore, we investigated the expression of γH2AX to further assess the anti-senescent role of USPBNPs. As shown, the mean fluorescence intensity of γ-H2AX in UVA-irradiated HDFs was strongly increased in comparison with non-irradiated HDFs, while USPBNP pretreatment significantly decreased the γ-H2AX expression in UVA-irradiated HDFs (Fig. 4A and B). The protein level of γ-H2AX in HDFs was also checked by western blot and a similar effect was observed. As shown, UVA irradiation significantly augmented the expression of γ-H2AX in HDFs, while USPBNP pretreatment decreased the γ-H2AX expression in UVA irradiated HDFs (Fig. 4C and D).

3.6 USPBNPs inhibit SASP secretion in UVA-irradiated human dermal fibroblasts

During the progress of cellular senescence, the secretion of proteins such as chemokines, inflammatory cytokines and proteases is increased.[32] These secreted proteins are known as SASP, which is also a major feature of cellular senescence.[17] The effect of USPBNPs on the expressions of several representative SASP including IL-6, TNF-α and MMPs in HDFs was studied. After UVA irradiation, the level of these proteins in HDFs was significantly increased (Fig. 5A and B). However, the expressions of these SASP were declined in the USPBNP pretreated HDFs compared to HDFs without USPBNP pretreatment (the UVA group). Thereafter, the transcriptional level of these SASP was also evaluated by q-RT PCR. Fig. 5C indicates that the mRNA levels of IL-6, TNF-α and MMPs in UVA-irradiated HDFs were significantly decreased by USPBNP pretreatment.

3.7 USPBNPs decrease the intracellular ROS level and inhibit the ERK/AP-1 pathway in UVA-irradiated human dermal fibroblasts

To investigate whether USPBNPs attenuated UVA-induced cellular senescence by scavenging intracellular ROS, we detected the level of ROS among different groups using a ROS assay kit. The fluorescence images captured using a confocal laser scanning microscope demonstrated that the mean fluorescence intensity of ROS in HDFs was remarkably higher after UVA radiation (Fig. 6A and B). However, pretreatment of USPBNPs significantly decreased the intracellular ROS level. The ROS-scavenging role of USPBNPs was also confirmed by flow cytometry as shown in Fig. 6C and D. Consistent with the above results, UVA radiation significantly increased the ROS level in HDFs compared to the control group while USPBNPs remarkably reduced the intracellular ROS level. As the ERK/AP-1 signaling cascade plays a crucial role in the ROS-mediated photoaging,[17] we next detected the level of key proteins in HDFs involved in the ERK/AP-1 pathway, including *p*-ERK, ERK, c-Jun and c-Fos. As shown, the ERK phosphorylation and expressions of downstream c-Jun and c-Fos in HDFs were significantly upregulated by UVA radiation compared with the control group (Fig. 6E and F). In contrast, USPBNP pretreatment significantly downregulated the ERK phosphorylation and expressions of c-Jun and c-Fos. Based on the above results, we deduced that USPBNPs alleviated UVA-induced cellular

senescence in HDFs by eliminating excessive ROS and inhibiting the ERK/AP-1 pathway.

4. Conclusions

In summary, 1 μg ml^{-1} of USPBNPs attenuate cellular senescence in UVA-irradiated HDFs by decreasing the SA-β-gal activity, inhibiting the G1/S phase arrest and senescence associated proteins, reducing the γ-H2AX expression and restraining the senescence associated secretory phenotype. Moreover, the anti-senescence effect of USPBNPs was mediated by diminishing excessive intracellular ROS through its nanozyme property and inhibiting the downstream ERK/AP-1 pathway. Considering the anti-cellular senescence effect of USPBNPs, we speculate that USPBNPs have great potential to serve as promising anti-photoaging agents.

Author contributions

Conflicts of interest

There are no conflicts to declare.

Acknowledgements

References

1 M. Wlaschek, I. Tantcheva-Poór, L. Naderi, W. Ma, L. A. Schneider, Z. Razi-Wolf, J. Schüller and K. Scharffetter-Kochanek, *J. Photochem. Photobiol., B*, 2001, **63**, 41–51.

2 M. Berneburg, H. Plettenberg and J. Krutmann, *Photodermatol., Photoimmunol. Photomed.*, 2000, **16**, 239–244.

3 G. J. Fisher, *Cutis*, 2005, **75**, 5–8; discussion 8-9.

4 E. Fitsiou, T. Pulido, J. Campisi, F. Alimirah and M. Demaria, *J. Invest. Dermatol.*, 2021, **141**, 1119–1126.

5 A. Kammeyer and R. M. Luiten, *Ageing Res. Rev.*, 2015, **21**, 16–29.

6 G. J. Fisher, Z. Q. Wang, S. C. Datta, J. Varani, S. Kang and J. J. Voorhees, *N. Engl. J. Med.*, 1997, **337**, 1419–1428.

7 L. Rittié and G. J. Fisher, *Ageing Res. Rev.*, 2002, **1**, 705–720.

8 J. Campisi and F. d'Adda di Fagagna, *Nat. Rev. Mol. Cell Biol.*, 2007, **8**, 729–740.

9 B. G. Childs, M. Gluscevic, D. J. Baker, R. M. Laberge, D. Marquess, J. Dananberg and J. M. van Deursen, *Nat. Rev. Drug Discovery*, 2017, **16**, 718–735.

10 X. Liu, Y. Gao, R. Chandrawati and L. Hosta-Rigau, *Nanoscale*, 2019, **11**, 21046–21060.

11 J. M. van Deursen, *Nature*, 2014, **509**, 439–446.

12 M. E. Waaijer, W. E. Parish, B. H. Strongitharm, D. van Heemst, P. E. Slagboom, A. J. de Craen, J. M. Sedivy, R. G. Westendorp, D. A. Gunn and A. B. Maier, *Aging Cell*, 2012, **11**, 722–725.

13 G. P. Dimri, X. Lee, G. Basile, M. Acosta, G. Scott, C. Roskelley, E. E. Medrano, M. Linskens, I. Rubelj, O. Pereira-Smith, *et al.*, *Proc. Natl. Acad. Sci. U. S. A.*, 1995, **92**, 9363–9367.

14 A. Calcinotto, J. Kohli, E. Zagato, L. Pellegrini, M. Demaria and A. Alimonti, *Physiol. Rev.*, 2019, **99**, 1047–1078.

15 L. J. Mah, A. El-Osta and T. C. Karagiannis, *Epigenetics*, 2010, **5**, 129–136.

16 D. M. Waldera Lupa, F. Kalfalah, K. Safferling, P. Boukamp, G. Poschmann, E. Volpi, C. Götz-Rösch, F. Bernerd, L. Haag, U. Huebenthal, E. Fritsche, F. Boege, N. Grabe, J. Tigges, K. Stühler and J. Krutmann, *J. Invest. Dermatol.*, 2015, **135**, 1954–1968.

17 M. Toutfaire, E. Bauwens and F. Debacq-Chainiaux, *Biochem. Pharmacol.*, 2017, **142**, 1–12.

18 C. López-Otín, M. A. Blasco, L. Partridge, M. Serrano and G. Kroemer, *Cell*, 2013, **153**, 1194–1217.

19 D. Jiang, D. Ni, Z. T. Rosenkrans, P. Huang, X. Yan and W. Cai, *Chem. Soc. Rev.*, 2019, **48**, 3683–3704.

20 Y. Huang, J. Ren and X. Qu, *Chem. Rev.*, 2019, **119**, 4357–4412.

21 J. Wu, X. Wang, Q. Wang, Z. Lou, S. Li, Y. Zhu, L. Qin and H. Wei, *Chem. Soc. Rev.*, 2019, **48**, 1004–1076.

22 Y. Huang, Z. Liu, C. Liu, Y. Zhang, J. Ren and X. Qu, *Chemistry*, 2018, DOI: 10.1002/chem.201801725.

23 N. Singh, M. A. Savanur, S. Srivastava, P. D'Silva and G. Mugesh, *Angew. Chem., Int. Ed. Engl.*, 2017, **56**, 14267–14271.

24 S. Li, L. Shang, B. Xu, S. Wang, K. Gu, Q. Wu, Y. Sun, Q. Zhang, H. Yang, F. Zhang, L. Gu, T. Zhang and H. Liu, *Angew. Chem., Int. Ed. Engl.*, 2019, **58**, 12624–12631.

25 D. F. Thompson and E. D. Callen, *Ann. Pharmacother.*, 2004, **38**, 1509–1514.

26 T. Wang, H. Dong, M. Zhang, T. Wen, J. Meng, J. Liu, Z. Li, Y. Zhang and H. Xu, *Nanoscale*, 2020, **12**, 23084–23091.

27 W. Zhang, S. Hu, J. J. Yin, W. He, W. Lu, M. Ma, N. Gu and Y. Zhang, *J. Am. Chem. Soc.*, 2016, **138**, 5860–5865.

28 Z. Qin, Y. Li and N. Gu, *Adv. Healthcare Mater.*, 2018, **7**, e1800347.

29 X. Xie, J. Zhao, W. Gao, J. Chen, B. Hu, X. Cai and Y. Zheng, *Theranostics*, 2021, **11**, 3213–3228.

30 A. Sahu, J. Jeon, M. S. Lee, H. S. Yang and G. Tae, *Mater. Sci. Eng., C*, 2021, **119**, 111596.

31 Z. Qin, B. Chen, Y. Mao, C. Shi, Y. Li, X. Huang, F. Yang and N. Gu, *ACS Appl. Mater. Interfaces*, 2020, **12**, 57382–57390.

32 J. P. Coppé, P. Y. Desprez, A. Krtolica and J. Campisi, *Annu. Rev. Phytopathol.*, 2010, **5**, 99–118.